

Non-existence of quantum black hole horizons in the improved dynamics approach

Wen-Cong Gan^{a,b,c} ^{*} Xiao-Mei Kuang^d [†] Zhen-Hao Yang^d [‡] Yungui Gong^e [§] Anzhong Wang^a [¶] and Bin Wang^{d,f} ^{**}

^a *GCAP-CASPER, Physics Department, Baylor University, Waco, Texas 76798-7316, USA*

^b *Institute for Theoretical Physics & Cosmology,*

Zhejiang University of Technology, Hangzhou, 310023, China

^c *United Center for Gravitational Wave Physics (UCGWP),*

Zhejiang University of Technology, Hangzhou, 310023, China

^d *Center for Gravitation and Cosmology, College of Physical Science*

and Technology, Yangzhou University, Yangzhou 225009, China

^e *School of Physics, Huazhong University of Science and Technology, Wuhan, Hubei 430074, China*

^f *School of Aeronautics and Astronautics, Shanghai Jiao Tong University, Shanghai 200240, China*

(Dated: February 7, 2023)

In this paper, we study the quantum geometric effects near the locations that black hole horizons used to appear in Einstein's classical theory within the framework of the improved dynamic approach, in which the two polymerization parameters of the Kantowski-Sachs spacetime are functions of the phase space variables. Our detailed analysis shows that the effects are so strong that black hole horizons of the effective quantum theory do not exist any longer, and the corresponding Kantowski-Sachs model now describes the entire spacetime of the trapped region, instead of being only the internal region of a black hole, as it is usually expected in loop quantum gravity.

I. INTRODUCTION

General relativity (GR) predicts its failure at spacetime singularities [1]. Two well known forms of singularities are the big-bang singularity in cosmology and the internal singularities of black holes. Quantum theories of gravity are expected to resolve these classical singularities by incorporating quantum effects, so the spacetimes near these singularities are still predictable quantum mechanically.

Loop quantum gravity (LQG) [2] is one of the promising candidates of quantum gravity, based on Hamiltonian formalism and canonical quantization of holonomies of the connection and the fluxes of the triads [3]. A very successful application of LQG is loop quantum cosmology (LQC) first considered in [4–6] and then completed in [7]. LQC is constructed by applying LQG techniques to cosmological models within the superminispace approach [6], and the resulting quantum corrections to classical geometry can be effectively described by semiclassical effective Hamiltonian that incorporate the leading-order quantum geometric effects [8]. The effective model works very well in comparison with the full quantum dynamics of LQC even in the deep quantum regime [9], especially for the states that are sharply peaked on a classical trajectory at late times [10]. LQC resolves the big-bang singularity because of the fundamental result of LQG: *quantum gravity effects always lead the area operator to have a non-zero minimal area gap* [2]. It is this non-zero

area gap that causes strong repulsive effects in the dynamics when the spacetime curvature reaches the Plank scale and the big-bang singularity is replaced by a quantum bounce [11].

In LQC, there exist two different quantization schemes, the so-called μ_o and $\bar{\mu}$ schemes, which give different representations of quantum Hamiltonian constraints and lead to different effective dynamics [9]. The fundamental difference of these two approaches rises in the implementation of the minimal area gap mentioned above. In the μ_o scheme, each holonomy $h_k^{(\mu)}$ is considered as an eigenstate of the area operator, associated with the face of the elementary cell orthogonal to the k -th direction. The parameter μ is fixed by requiring the corresponding eigenvalue be the minimal area gap. As a result, μ is a constant in this approach [6]. However, it has been shown [12] that this quantization does not have a proper semiclassical limit, and suffers from the dependence on the length of the fiducial cell. It also lacks of consistent identified curvature scales. On the other hand, in the $\bar{\mu}$ scheme [7], the quantization of areas is referred to the physical geometries, and when shrinking a loop until the minimal area enclosed by it, one should use the physical geometry. Since the latter depends on the phase space variables, now when calculating the holonomy $h_k^{(\mu)}$, one finds that the parameter μ depends on the phase space variables, too. In the literature, this improved dynamical approach is often referred to as the $\bar{\mu}$ scheme, and has been shown to be the only scheme discovered so far that overcomes the limitations of the μ_o scheme and is consistent with observations [9].

In parallel to the studies of LQC, loop quantum black holes (LQBHs) have been also intensively studied in the past decade or so (See, for example, [13–17] and references therein). In particular, since the Schwarzschild black hole interior can be treated as the Kantowski-Sachs cosmological model, in which the spacetime is homoge-

^{*} Wen-cong.Gan1@baylor.edu

[†] xmeikuang@yzu.edu.cn

[‡] yangzhenhao.yzu@163.com

[§] yggong@hust.edu.cn

[¶] Anzhong_Wang@baylor.edu; Corresponding author

^{**} wang_b@sjtu.edu.cn

neous and the metric is only time-dependent, some of the LQC techniques can be borrowed to study the black hole interiors directly. Along this line of thinking, LQBHs were initially studied within the μ_o scheme [18–20]. However, this LQBH model also suffers from similar limitations as the μ_o scheme in LQC [14, 21, 22]. Soon the $\bar{\mu}$ scheme was applied to the Schwarzschild black hole interior by Böhmer and Vandersloot (BV) [23] (See also [24, 25] for a similar prescription in the Kantowski-Sachs universe, and [26–31] in the Painlevé-Gullstrand-like coordinates that cover both of the internal and external regions of the classical Schwarzschild black hole.¹). Later, the $\bar{\mu}$ quantization scheme was shown to be the unique quantization scheme that is free from the dependence on the fiducial length and has consistent ultraviolet and infrared behavior [37]. It was also shown that it has universally bounded curvature scales and energy density, and that the expansion and shear scalars are all finite, in addition to the geodesic completeness and generic resolution of strong singularities [38].

Despite of these attractive features, the BV model suffers a severe drawback: *there are large departures from the classical theory very near the classical black hole horizon even for massive black holes, for which the curvatures at the horizon become very low* [14, 21–23]. In addition, when the curvature reaches the Planck scale, the geometric radius of the round 2-spheres researches a minimum and then bounces, giving rise to a transition surface \mathcal{T} , whereby the original singularity is replaced by a quantum bounce. The transition surface \mathcal{T} naturally divides the spacetime into two regions. To the past of \mathcal{T} we have a trapped region, and to its future an anti-trapped region appears, in which the geometric radius of the 2-spheres increases. However, in contrast to other LQBH models, this anti-trapped region is not bounded by a white-hole-like horizon, instead it is followed by another bounce, across which the region becomes trapped again, and the radius of the 2-spheres starts to decrease [23–25]. This process will be repeating indefinitely, and after each bounce the geometric radius of the 2-spheres will get smaller. So, soon the area of the 2-spheres will become smaller than the minimal area gap, whereby the model becomes self-inconsistent [14].

In this paper, we shall mainly focus our attention to the past of \mathcal{T} , as the spacetimes in the pre-transition phase were already studied in detail first in the vacuum case [23–25] and then in the case filled with matter [37] or a cosmological constant [39]. In all the cases, the spacetimes approach to the classical “charged” Nariai solutions, in which the radii of the two-spheres become constants asymptotically, but with values smaller than the Planck scale. So, the validity of this asymptotic behavior is questionable [14]. In this paper, we shall put this ques-

tion aside, and study in detail the spacetimes to the past of \mathcal{T} by focusing ourselves onto the quantum geometric effects near the location that the classical black horizon used to appear, especially the possible development of black hole horizons [1, 14, 40–42]. To our surprising, we find that such a horizon is never developed within a finite time. Thus, in the BV model the quantum geometric effects are so strong that the black hole horizon used to appear classically at $T_H \equiv \ln(2m)$ now disappears, and the resultant Kantowski-Sachs model covers already the entire spacetime to the past of the transition surface \mathcal{T} [38]. As a result, the external region of a quantum black hole in this model does not exist.

Specifically, the paper is organized as follows: In Sec. II we first give a brief introduction to the internal region of the classical Schwarzschild black hole, whereby obtain the classical Hamiltonian with a special choice of the lapse function. Then, an effective loop quantum Hamiltonian can be obtained within the framework of the superminispace quantization scheme [6], by replacing the two canonical phase space variables b and c via the relations

$$b \rightarrow \frac{\sin(\delta_b b)}{\delta_b}, \quad c \rightarrow \frac{\sin(\delta_c c)}{\delta_c},$$

in the classical lapse function and Hamiltonian, where δ_b and δ_c are the two polymerization parameters, which are in general functions of the phase space variables. With the general choice of δ_b and δ_c , the dynamical equations are given by Eqs.(2.28) - (2.31).

In Sec. III, we consider the BV model by first introducing the BV prescription of the two polymerization parameters δ_b and δ_c given by Eq.(3.3), and then write down the corresponding dynamical equations, given explicitly by Eqs.(3.6) - (3.9). To estimate the region where the quantum effects near the classical black hole horizon become important, we first introduce a parameter ϵ via the relation $T_\epsilon = T_H(1 - \epsilon)$ at which $|\delta_c c|_{T_\epsilon} \simeq \mathcal{O}(1)$, from which we find that such effects become important only very closed to T_H for massive black holes. To study such effects explicitly, the choice of initial time and conditions are crucial. In this paper we choose the initial time T_i that is far from both the transition surface and the classical black horizon, $T_\mathcal{T} \ll T_i \ll T_H$, so that the initial conditions are as closed to those of classical theory as possible [cf. Table II]. With these initial conditions we study the evolution of the dynamical equations, and find that the metric coefficients remain finite and non-singular within any given finite time. These results are strongly supported by the analytical studies carried out in [38]. In particular, it was shown explicitly that $0 < p_b(\tau), p_c(\tau) < \infty$ at any given finite time τ , where p_b and p_c are the metric coefficients defined in Eq.(2.1), and τ denotes the proper time, obtained by setting the lapse function to be unity. Then, we turn to study the existence of marginally trapped surfaces by analyzing the expansions of the in-going and out-going radially-moving light rays, as well as the normal vector to the

¹ For rigorous mathematical development of Ashtekar’s formalism for spherically symmetric general minispaces and its loop quantization, see, for example, [28, 32–36] and references therein.

two-spheres, and find that such surfaces indeed exist. However, they represent neither black hole horizons nor white hole ones, as they always separate trapped regions from anti-trapped ones, or vice versa, instead of separating trapped (anti-trapped) regions from untrapped ones, as a black (white) hole horizon usually does [1, 14, 40–42]. Finally, in Sec. IV, we present our main conclusions.

Before proceeding to the next section, we note the following: In this paper the Planck length ℓ_{pl} and mass M_{pl} are defined, respectively, by $\ell_{pl} \equiv \sqrt{G\hbar/c^3}$ and $M_{pl} \equiv \sqrt{\hbar c/G}$, where G denotes the Newtonian constant, \hbar is the Planck constant divided by 2π , and c is the speed of light (Note that in the main text, c will be used to denote a phase space variable, and only in this paragraph we use it to denote the speed of light, without causing any confusion.). Thus, in terms of the fundamental units, M , L and T , the units of \hbar and c are $[\hbar] = ML^2T^{-1}$, $[c] = LT^{-1}$, where M , L and T denote the units of mass, length and time, respectively. In this paper we shall adopt the natural units, so that $\hbar = c = 1$. Then, we find $L = T$, $M = L^{-1}$, $[G] = L^3M^{-1}T^{-2} = L^2$. In addition, all the figures will be plotted in the units of ℓ_{pl} and M_{pl} , whenever the length and mass parameters are involved.

II. INTERNAL SPACETIMES OF LOOP QUANTUM BLACK HOLES

The internal spacetime of a spherically symmetric black hole can always be written in the Kantowski-Sachs form

$$ds^2 = -N^2dT^2 + \frac{p_b^2}{L_o^2 |p_c|} dx^2 + |p_c| d\Omega^2, \quad (2.1)$$

where N , p_b , p_c are all functions of T only, L_o denotes the length of the fiducial cell in the x -direction, and $d\Omega^2 \equiv d\theta^2 + \sin^2\theta d\phi^2$. The function N is often called the lapse function, and p_b and p_c are the dynamical variables, which satisfy the Poisson brackets

$$\{c, p_c\} = 2G\gamma, \quad \{b, p_b\} = G\gamma, \quad (2.2)$$

where γ is the Barbero-Immirzi parameter, and b and c are the corresponding phase space conjugate momenta of p_b and p_c , respectively. The dimensions of the four phase space variables ($p_b, b; p_c, c$) are

$$[p_b] = [p_c] = L^2, \quad [b] = [c] = 1, \quad (2.3)$$

with $[x] = [L_o] = L$, where “1” now means dimensionless. The dimension of the coordinate T depends on the choice of the gauge. In particular, for the gauge of Eq.(2.8) given below, the lapse function has the dimension of length, while T is dimensionless, i.e.

$$[N^{\text{GR}}] = L, \quad [T] = 1. \quad (2.4)$$

It should be noted that the Kantowski-Sachs metric

(2.1) is invariant under the gauge transformations

$$T = f(\hat{T}), \quad x = \alpha\hat{x} + x_o, \quad (2.5)$$

via the redefinitions of the lapse function and the length of the fiducial cell,

$$\hat{N} = Nf_{,\hat{T}}, \quad \hat{L}_o = \frac{L_o}{\alpha}, \quad (2.6)$$

where $f(\hat{T})$ is an arbitrary function of \hat{T} , and α and x_o are constants. The equations of motions (EoMs) of the system can be obtained from the Hamiltonian equations,

$$\frac{dA}{dT} = \{A, H\}, \quad (2.7)$$

for any physical variable A of the system.

A. Classical Model

To facilitate our discussions of LQBHs, let us first briefly review the classical black hole solution in Einstein’s theory of general relativity (GR). It is convenient to choose the lapse function as

$$N^{\text{GR}} = \frac{\gamma \operatorname{sgn}(p_c) |p_c|^{1/2}}{b}, \quad (2.8)$$

which can be always realized by the gauge freedom of Eq.(2.5) without loss of the generality. Then, the corresponding Hamiltonian is given by [14]

$$\begin{aligned} H^{\text{GR}}[N^{\text{GR}}] &\equiv N^{\text{GR}} \mathcal{H}^{\text{GR}} \\ &= -\frac{1}{2G\gamma} \left(2c p_c + \left(b + \frac{\gamma^2}{b} \right) p_b \right). \end{aligned} \quad (2.9)$$

Thus, from Eq.(2.7) we find

$$\dot{b} = \{b, H^{\text{GR}}\} = G\gamma \frac{\partial H^{\text{GR}}}{\partial p_b} = -\frac{1}{2b} (b^2 + \gamma^2), \quad (2.10)$$

$$\dot{c} = \{c, H^{\text{GR}}\} = 2G\gamma \frac{\partial H^{\text{GR}}}{\partial p_c} = -2c, \quad (2.11)$$

$$\dot{p}_b = \{p_b, H^{\text{GR}}\} = -G\gamma \frac{\partial H^{\text{GR}}}{\partial b} = \frac{p_b}{2b^2} (b^2 - \gamma^2), \quad (2.12)$$

$$\dot{p}_c = \{p_c, H^{\text{GR}}\} = -2G\gamma \frac{\partial H^{\text{GR}}}{\partial c} = 2p_c, \quad (2.13)$$

where an overdot denotes the derivative with respect to T . Then, the integrations of Eqs.(2.10), (2.11) and (2.13) yield, respectively

$$b^{\text{GR}}(T) = \pm \gamma \sqrt{e^{T_o - T} - 1}, \quad (2.14)$$

$$c^{\text{GR}}(T) = c_o e^{-2T}, \quad (2.15)$$

$$p_c^{\text{GR}}(T) = p_c^o e^{2T}, \quad (2.16)$$

where T_o , c_o and p_c^o are three integration constants with T_o and c_o being dimensionless and p_c^o of dimensions of L^2 .

TABLE I. Different choices of the quantum parameters δ_b and δ_c for different quantization schemes.

	μ_0	$\bar{\mu}'$	CS	AOS	$\bar{\mu}$	ABP	Modesto	BMM	GM
δ_b	$4\sqrt{3}$	$\sqrt{\frac{\Delta}{p_b}}$	$\frac{\sqrt{\Delta}}{r_o}$	$\left(\frac{\sqrt{\Delta}}{\sqrt{2\pi\gamma^2}m}\right)^{1/3}$	$\sqrt{\frac{\Delta}{p_c}}$	$\frac{\alpha}{R} = \frac{\alpha}{ p_c ^{1/2}}$	$\sigma(\delta)\delta$	$f(O_b)$	$f_b(O_b, O_c)$
δ_c	$4\sqrt{3}$	$\sqrt{\frac{\Delta}{p_c}}$	$\frac{\sqrt{\Delta}}{L_o}$	$\frac{1}{2L_o} \left(\frac{\gamma\Delta^2}{4\pi^2m}\right)^{1/3}$	$\frac{\sqrt{\Delta}p_c}{p_b}$	$\frac{\beta}{\Lambda} = \frac{\beta p_c ^{1/2}}{p_b}$	δ	$f(O_c)$	$f_b(O_b, O_c)$
	[19]	[25]	[21]	[14, 43]	[23]	[44–46]	[47–50]	[51, 52]	[52, 53]

To find p_b , we can first substitute the above solutions to Eq.(2.12) and then integrate it to find p_b , which will yield an additional integration constant, say, p_b^o . But, this constant is not arbitrary and must be chosen so that the classical Hamiltonian given by Eq.(2.9) vanishes identically. A more straightforward way is to submit the above solutions into the classical Hamiltonian Eq.(2.9) and find p_b directly from this constraint. In doing so, we obtain

$$p_b^{\text{GR}}(T) = \mp \frac{2c_o p_c^o}{\gamma} e^{T-T_o} \sqrt{e^{T_o-T} - 1}. \quad (2.17)$$

Hence, we have

$$N^{\text{GR}} = \pm \frac{\text{sgn}(p_c) |p_c^o|^{1/2}}{\sqrt{e^{T_o-T} - 1}} e^T, \quad (2.18)$$

and

$$ds^2 = |p_c^o| \left(-\frac{e^{2T}}{e^{T_o-T} - 1} dT^2 + \frac{4c_o^2 e^{-2T_o}}{\gamma^2 L_o^2} (e^{T_o-T} - 1) dx^2 + e^{2T} d\Omega^2 \right). \quad (2.19)$$

Thus, without loss of the generality, we can always assume $p_c^o > 0$. Then, setting $r = \sqrt{p_c^o} e^T$ and rescaling x by

$$x \rightarrow t \equiv -\frac{2c_o \sqrt{p_c^o} e^{-T_o}}{\gamma L_o} x, \quad (2.20)$$

the above metric takes the form of the classical Schwarzschild solution

$$ds^2 = -\frac{1}{\frac{2m}{r} - 1} dr^2 + \left(\frac{2m}{r} - 1 \right) dt^2 + r^2 d\Omega^2 \quad (2.21)$$

with $r < 2m$, where $m \equiv \sqrt{p_c^o} e^{T_o}/2$, related to the mass of the black hole via the relation $M = m/G$. Thus, the parameter m has the dimension, $[m] = M^{-1} = L$ for the units adopted in this paper.

From the above analysis, we can see that the rescaling (2.20) simply allows us to set

$$\frac{2c_o \sqrt{p_c^o} e^{-T_o}}{\gamma L_o} = -1. \quad (2.22)$$

On the other hand, using the gauge residual $T \rightarrow \hat{T} = T + C_o$, we can always set $p_c^o = 1$, where $C_o \equiv (1/2) \ln p_c^o$. Certainly, this rescaling will lead to $T - T_o = \hat{T} - \hat{T}_o$ and $m \equiv \sqrt{p_c^o} e^{T_o}/2 = e^{\hat{T}_o}/2$, where $\hat{T}_o \equiv T_o + C_o$. In addition, L_o does not appear in the dynamical equations (2.10) - (2.13). Therefore, without loss of the generality, we can always set $L_o = 1$. In summary, the constants p_c^o , c_o and L_o can be chosen as

$$p_c^o = 1, \quad L_o = 1, \quad c_o = -\frac{\gamma L_o e^{T_o}}{2\sqrt{p_c^o}} = -\gamma m, \quad (2.23)$$

without affecting the physics of the spacetimes of the corresponding dynamical equations. Hence, we obtain

$$\begin{aligned} b^{\text{GR}}(T) &= \pm \gamma \sqrt{2m e^{-T} - 1}, \\ p_b^{\text{GR}}(T) &= \pm e^T \sqrt{2m e^{-T} - 1}, \\ c^{\text{GR}}(T) &= -\gamma m e^{-2T}, \quad p_c^{\text{GR}}(T) = e^{2T}. \end{aligned} \quad (2.24)$$

In the rest of this paper, without loss of the generality, we shall choose the “+” signs for both $b^{\text{GR}}(T)$ and $p_b^{\text{GR}}(T)$.

It is interesting to note that there is essentially only one physical parameter m that determines the properties of the classical spacetime, while the parameter γ affects only the dynamical equations through Eqs.(2.10) - (2.13), but has no effects on the spacetime. This is true only classically, and quantum mechanically γ does affect the properties of quantum spacetimes. In particular, the considerations of black hole thermodynamics in LQG requires $\gamma \simeq 0.2375$ [54].

B. Effective Loop Quantum Black Holes

In LQC, the leading order quantum corrections are incorporated by introducing quantum parameters δ_b and δ_c which stand for *edge length* of holonomy. This procedure is called polymerization [19]. And the resultant quantum corrected spacetime can be obtained from the effective Hamiltonian. Because the Schwarzschild black hole interior can be treated as a Kantowski-Sachs cosmological model, polymerization can be used to construct the effective Hamiltonian which describes the interior of a quantum black hole. Polymerization is realized by the

replacements [19]

$$b \rightarrow \frac{\sin(\delta_b b)}{\delta_b}, \quad c \rightarrow \frac{\sin(\delta_c c)}{\delta_c}, \quad (2.25)$$

in the classical lapse function N^{GR} (2.8) and Hamiltonian H^{GR} (2.9), so that we obtain

$$N^{\text{eff}} = \frac{\gamma \delta_b \sqrt{p_c}}{\sin(\delta_b b)}, \quad (2.26)$$

$$H^{\text{eff}}[N^{\text{eff}}] = -\frac{1}{2\gamma G} \left[2 \frac{\sin(\delta_c c)}{\delta_c} p_c + \left(\frac{\sin(\delta_b b)}{\delta_b} + \frac{\gamma^2 \delta_b}{\sin(\delta_b b)} \right) p_b \right]. \quad (2.27)$$

Note that in writing the above expressions, we had assumed $p_c > 0$ without loss of the generality, as shown above. Eqs.(2.26) and (2.27) will reduce, respectively, to the classical expressions of Eqs.(2.8) and (2.9) in the limit $\delta_b \rightarrow 0$ and $\delta_c \rightarrow 0$.

Depending on the models, δ_b and δ_c can be chosen as constants or functions of the phase-space variables (p_b, p_c, b, c) . Different choices correspond to different quantization scheme and lead to different effective dynamics. Some of them suffer from dependence on fiducial cell [19, 25], and some suffer from large quantum effects in low curvature regions [23]. We list some of the models considered so far in Table. I, and for more details, see, for example, [13–17] and references therein.

Assuming that δ_b and δ_c depend only on p_b and p_c [cf. Table. I], the EoMs corresponding to the above effective Hamiltonian are given by

$$\dot{b} = G\gamma \frac{\partial H^{\text{eff}}}{\partial p_b} = -\frac{1}{2} \left\{ 2 \left(\frac{c \cos(\delta_c c)}{\delta_c} - \frac{\sin(\delta_c c)}{\delta_c^2} \right) \frac{\partial \delta_c}{\partial p_b} p_c + \left[\frac{\gamma^2 \delta_b}{\sin(\delta_b b)} + \frac{\sin(\delta_b b)}{\delta_b} \right] + p_b \frac{\partial}{\partial p_b} \left[\frac{\gamma^2 \delta_b}{\sin(\delta_b b)} + \frac{\sin(\delta_b b)}{\delta_b} \right] \right\}, \quad (2.28)$$

$$\dot{c} = 2G\gamma \frac{\partial H^{\text{eff}}}{\partial p_c} = - \left\{ 2 \left(\frac{c \cos(\delta_c c)}{\delta_c} - \frac{\sin(\delta_c c)}{\delta_c^2} \right) \frac{\partial \delta_c}{\partial p_c} p_c + 2 \frac{\sin(\delta_c c)}{\delta_c} + p_b \frac{\partial}{\partial p_c} \left[\frac{\gamma^2 \delta_b}{\sin(\delta_b b)} + \frac{\sin(\delta_b b)}{\delta_b} \right] \right\}, \quad (2.29)$$

$$\dot{p}_c = -2G\gamma \frac{\partial H^{\text{eff}}}{\partial c} = 2p_c \cos(\delta_c c), \quad (2.30)$$

$$\dot{p}_b = -G\gamma \frac{\partial H^{\text{eff}}}{\partial b} = \frac{p_b}{2} \cos(\delta_b b) \left[1 - \frac{\gamma^2 \delta_b^2}{\sin^2(\delta_b b)} \right]. \quad (2.31)$$

As mentioned above, when $|\delta_b b|$ and $|\delta_c c|$ are small, $H^{\text{eff}}[N^{\text{eff}}]$ will reduce to $H^{\text{GR}}[N^{\text{GR}}]$. Conversely, the quantum effects become significant when $|\delta_b b| \sim \mathcal{O}(1)$ and/or $|\delta_c c| \sim \mathcal{O}(1)$ [23, 25]. In this paper we will mainly focus on the so-called $\bar{\mu}$ scheme first proposed in [23]. In LQC, this is the only scheme that leads to a consistent quantum cosmological model [7, 9].

III. BÖHMER-VANDERSLOOT MODEL

In LQC, the consistent prescription for the polymerization parameters were obtained by requiring that the physical area $A_{x\theta} (= \delta_b \delta_c p_b)$ [7] ² of the closed holonomy loop in the (x, θ) -plane is equal to the minimum area gap

predicted by LQG, $\Delta \equiv 4\sqrt{3}\pi\gamma\ell_{pl}^2$, so that

$$\delta_b \delta_c p_b = \Delta. \quad (3.1)$$

However, for the holonomies on the two-sphere, the loop does not close, and BV requires that $A_{\theta\phi} (= \delta_b^2 p_c)$ be equal to the minimum area, i.e.

$$\delta_b^2 p_c = \Delta. \quad (3.2)$$

Then, from the above equations we find

$$\delta_b = \sqrt{\frac{\Delta}{p_c}}, \quad \delta_c = \frac{\sqrt{\Delta p_c}}{p_b}, \quad (3.3)$$

which are all dimensionless and often referred to as the $\bar{\mu}$ -scheme for the spherically symmetric spacetimes [23]. Hence, we have

$$\frac{\partial \delta_b}{\partial p_b} = 0, \quad \frac{\partial \delta_b}{\partial p_c} = -\frac{\delta_b}{2p_c}, \quad (3.4)$$

$$\frac{\partial \delta_c}{\partial p_b} = -\frac{\delta_c}{p_b}, \quad \frac{\partial \delta_c}{\partial p_c} = \frac{\delta_c}{2p_c}. \quad (3.5)$$

² In the homogeneous isotropic universe, we have $\delta_b = \delta_c \equiv \delta$. As a result, the condition (3.1) uniquely determines δ . But, in the Kantowski-Sachs spacetime, this is no longer the case. So, in general we have $\delta_b \neq \delta_c$, and now one more condition is needed, in order to determine both δ_b and δ_c uniquely.

Inserting them into Eqs.(2.28) - (2.31), we obtain

$$\dot{b} = -\frac{c\mathcal{F}}{2\frac{\sin(\delta_c c)}{\delta_c}} \cos(\delta_c c), \quad (3.6)$$

$$\begin{aligned} \dot{c} = & -\frac{\frac{\sin(\delta_c c)}{\delta_c}}{\mathcal{F}} \left\{ b \cos(\delta_b b) - b \cos(\delta_b b) \frac{\gamma^2 \delta_b^2}{\sin^2(\delta_b b)} \right. \\ & \left. + 2 \frac{\gamma^2 \delta_b}{\sin(\delta_b b)} \right. \\ & \left. + \delta_c c \cot(\delta_c c) \left[\frac{\gamma^2 \delta_b}{\sin(\delta_b b)} + \frac{\sin(\delta_b b)}{\delta_b} \right] \right\}, \end{aligned} \quad (3.7)$$

$$\dot{p}_c = 2p_c \cos(\delta_c c), \quad (3.8)$$

$$\dot{p}_b = \frac{p_b}{2} \cos(\delta_b b) \left[1 - \frac{\gamma^2 \delta_b^2}{\sin^2(\delta_b b)} \right], \quad (3.9)$$

where

$$\mathcal{F} \equiv \frac{\gamma^2 \delta_b}{\sin(\delta_b b)} + \frac{\sin(\delta_b b)}{\delta_b}. \quad (3.10)$$

After taking the following identity into account

$$\frac{p_c}{p_b} = \frac{\delta_c}{\delta_b} = -\frac{\mathcal{F}}{2\frac{\sin(\delta_c c)}{\delta_c}}, \quad (3.11)$$

it can be shown that Eqs.(3.6)-(3.9) reduce to Eqs.(58)-(61) given in [23]. In particular, now the effective Hamiltonian (2.27) takes the form

$$\begin{aligned} H^{\text{eff}}[N^{\text{eff}}] &= -\frac{p_c}{2\gamma G \sin(\delta_b b) \delta_c} C_{\text{BV}}, \\ C_{\text{BV}} &\equiv 2 \sin(\delta_b b) \sin(\delta_c c) + \sin(\delta_b b)^2 + \gamma^2 \delta_b^2. \end{aligned} \quad (3.12)$$

A. Quantum Effects Near the Classical Black Hole Horizon

The classical black hole horizon is located at

$$T_H = \ln(2m), \quad (3.13)$$

as can be seen clearly from Eq.(2.24), at which we have $p_b^{\text{GR}} = 0$. Before solving the EoMs, let us first estimate the quantum effects near $T = T_H$. Substituting the classical Schwarzschild black hole solution given by Eqs.(2.14)-(2.17) into Eq.(3.3), we find

$$|\delta_b b| = \frac{\sqrt{\Delta}}{e^T} \gamma \sqrt{2me^{-T} - 1} \rightarrow 0, \quad T \rightarrow T_H, \quad (3.14)$$

but

$$|\delta_c c| = \frac{\sqrt{\Delta} \gamma m e^{-2T}}{\sqrt{2me^{-T} - 1}} \rightarrow \infty, \quad T \rightarrow T_H. \quad (3.15)$$

Eq.(3.15) indicates that the BV solution has large quantum effects near $T \simeq T_H$. To characterize these ef-

fects, in the vicinity of T_H let us introduce ϵ through $T = T_\epsilon \equiv T_H(1 - \epsilon)$ with $\epsilon \ll 1$. Then, assuming that at T_ϵ we have $|\delta_c c(T_\epsilon)| \simeq \mathcal{O}(1)$, so that

$$\begin{aligned} |\delta_c c|_{T=T_\epsilon} &= \frac{\sqrt{\Delta} \gamma m e^{-2T_\epsilon}}{\sqrt{2me^{-T_\epsilon} - 1}} \approx \frac{\sqrt{\Delta} \gamma m e^{-2T_H}}{\sqrt{2me^{-T_\epsilon} - 1}} \\ &\approx \frac{\sqrt{\Delta} \gamma}{4m \sqrt{(2m)^\epsilon - 1}} \sim \mathcal{O}(1), \end{aligned} \quad (3.16)$$

which leads to

$$\epsilon \simeq \frac{\ln(\frac{\Delta \gamma^2}{16m^2} + 1)}{\ln(2m)}. \quad (3.17)$$

From this expression we can see that as m increases, ϵ decreases sharply, that is, we need to get very close to T_H in order to see the quantum effects for massive black holes. In fact, in the following we shall show that such quantum effects are so large that the horizon is never formed within a finite time T . Recall that the geometric radius r of the two spheres $T, x = \text{constant}$ now is given by $r = e^T$. This in turn implies that in the BV approach quantum black hole horizons do not exist in the whole trapped region, $T > T$, with the only exception: it might be possible to exist at $r = \infty$ (or $T = \infty$).

B. Initial Conditions

To show our above claim, let us first consider the initial conditions. Since Eqs.(3.6) - (3.9) are four first-order ordinary differential equations, four initial conditions in general are needed. However, these initial conditions must also satisfy the Hamiltonian constraint $H^{\text{eff}} = 0$, so only three of them are independent. As a result, the phase space of the initial conditions is three-dimensional (3D). Without loss of the generality, we can first choose the initial conditions for $p_b(T_i)$, $p_c(T_i)$ and $b(T_i)$ at the initial time $T = T_i$, and then solve the effective Hamiltonian constraint to find $c(T_i)$. It is clear that such obtained 3D phase space includes all the possible real values of $p_b(T_i)$, $p_c(T_i)$ and $b(T_i)$. However, to compare the resultant BV spacetimes with the Schwarzschild one, we choose them as their corresponding values of GR, that is

$$\begin{aligned} p_b(T_i) &= p_b^{\text{GR}}(T_i), & p_c(T_i) &= p_c^{\text{GR}}(T_i), \\ b(T_i) &= b^{\text{GR}}(T_i), \end{aligned} \quad (3.18)$$

and

$$H^{\text{eff}}(T_i) = 0 \Rightarrow c(T_i) = c^{\text{eff}}(T_i). \quad (3.19)$$

Once the initial conditions are chosen at a chosen initial time T_i , the EoMs Eqs.(3.6)-(3.9) will uniquely determine the four physical variables (p_b, b, p_c, c) at any given later time T .

Due to the large quantum effects near T_H as estimated in the last subsection, normally we choose T_i far from

TABLE II. Initial values of $c(T_i)$ calculated from Eq.(3.19) at different times T_i and the corresponding classical values $c^{\text{GR}}(T_i)$ for $m = M/G = \ell_{pl}$, for which we have $T_{\mathcal{T}} \simeq -1.49$ and $T_H \simeq 0.693$.

T_i	-1.45	0.3	0.643	0.685
$c(T_i)$	2.68044 - 2.09266 I	-0.13272	-0.0682837	-0.0883704 + 0.0213373 I
$c^{\text{GR}}(T_i)$	-4.31636	-0.130343	-0.0656195	-0.0603504

T_H , that is, $T_i \ll T_H$ ³. On the other hand, near the throat $T = T_{\mathcal{T}}$ it is expected that the spacetime geometry will be dramatically different from that of GR, so the conditions given by Eq.(3.18) near $T_{\mathcal{T}}$ might not hold. Therefore, in general we choose T_i so that

$$T_{\mathcal{T}} \ll T_i \ll T_H. \quad (3.20)$$

To understand the above arguments further, we consider the initial conditions at different times T_i 's. We compare the effective value of $c(T_i) = c^{\text{eff}}(T_i)$ obtained from Eq.(3.19) with its corresponding classical value $c^{\text{GR}}(T_i)$ at different times T_i 's in Table II for $m = \ell_{pl}$, for which we have $T_{\mathcal{T}} \simeq -1.49$, and $T_H \simeq 0.693$. From the Table we can see that Eq.(3.19) has no real-value solutions for $c(T_i)$ when T_i is very closed to either the transition surface $T_{\mathcal{T}}$ or to the classical horizon T_H , which means that the quantum effects are so large near these points, so that the effective Hamiltonian constraint Eq.(3.19) has no physical solutions for such chosen $p_b(T_i)$, $p_c(T_i)$ and $b(T_i)$. On the other hand, when far away from these points, the difference between $c(T_i)$ and $c^{\text{GR}}(T_i)$ is small. Therefore, in the following, we shall choose T_i so that the condition (3.20) is always satisfied.

C. Numerical Results

Once the initial time and conditions are specified, we are ready to solve EoMs (3.6) - (3.9) numerically. To monitor the numerical errors, we shall closely pay attention to the effective Hamiltonian given by Eq.(3.12), which is required to vanish identically

$$H^{\text{eff}} \simeq 0, \quad (3.21)$$

along any of physical trajectories. However, numerically this is true only up to certain accuracy. To make sure

that such numerical calculations are reliable, and our physical conclusions will not depend on these numerical errors, we run our *Mathematica* code in supercomputers with high precisions. In particular, in all calculations we require that the Working Precision and Precision Goal be respectively 250 and 245, where Working Precision specifies how many digits of precisions should be maintained in internal computations of *Mathematica*, and Precision Goal specifies how many effective digits of precisions should be sought in the final result.

1. Asymptotic Behavior of the Spacetimes as $T \gg T_{\mathcal{T}}$

With the above in mind, let first consider the case $m = \ell_{pl}$. In this case, we have $T_{\mathcal{T}} \simeq -1.49$ and $T_H \simeq 0.693$. The initial point is chosen at $T_i = 0.3$, which satisfies Eq.(3.20). From Table II we can also see that at this point $c(T_i)$ is very closed to its corresponding classical value $c^{\text{GR}}(T_i)$. In Fig. 1 we plot all the four variables b , c , p_b and p_c , together with H^{eff} , the corresponding Kretschmann scalar K and the metric components N^2 and g_{xx} , where the Kretschmann scalar K is defined as $K(T) \equiv R_{\alpha\beta\mu\nu}R^{\alpha\beta\mu\nu}$. From Fig. 1 (h) we can see that the maximal errors happen near $T \simeq 10$ at which $|H^{\text{eff}}| \leq 2.0 \times 10^{-8}$. Before or after it, we have $|H^{\text{eff}}| \ll 10^{-8}$. Therefore, our numerical computations are reliable.

On the other hand, from Fig. 1 (d) we can see that the geometric radius $r = \sqrt{p_c}$ is exponentially increasing. As a result, the metric coefficient g_{xx} decreases exponentially, but never be zero precisely for any given finite time T , as shown by Fig. 1 (f). In addition, the lapse function square N^2 is also oscillating with a similar period as that of p_b , but after each circle of oscillations it is getting larger and larger [cf. Fig. 1 (e)]. However, it always remains finite. Moreover, in Fig. 1 (g) we plot out the Kretschmann scalar $K(T)$ together with its classical counterpart $K^{\text{GR}}(T) \equiv 48m^2/p_c^3$, from which we can see clearly that the quantum geometric effects indeed become very large near the location of the classical black hole horizon $T \simeq \ln(2m)$. This deviation lasts for a quite while [$T \in (T_H, 160)$ for $m = \ell_{pl}$], but finally $K(T)$ will be decreasing as p_c^{-3} , the same as $K^{\text{GR}}(T)$, that is,

$$K(T) \simeq \frac{K_0}{p_c^3}, \quad K_0 > 48m^2, \quad (3.22)$$

as $T \rightarrow \infty$. But, we always have $K_0 > 48m^2$.

³ It should be noted that $c(T_i) = c^{\text{eff}}(T_i)$ obtained from $H^{\text{eff}}(T_i) = 0$ can still be significantly different from $c^{\text{GR}}(T_i)$, even $T_i \simeq T_H$ and $p_b(T_i)$, $p_c(T_i)$ and $b(T_i)$ are chosen as their corresponding values of GR, as given by Eq.(3.18), because now $H^{\text{eff}}(T_i) \neq H^{\text{GR}}(T_i)$. In fact, from Eq.(3.15) we find that $|\delta_c c|$ is still very large near T_H , precisely because the fact that now $c(T_i)$ still deviates from its classical value significantly. Then, the solution cannot be approximated by the classical Schwarzschild black hole at T_H .

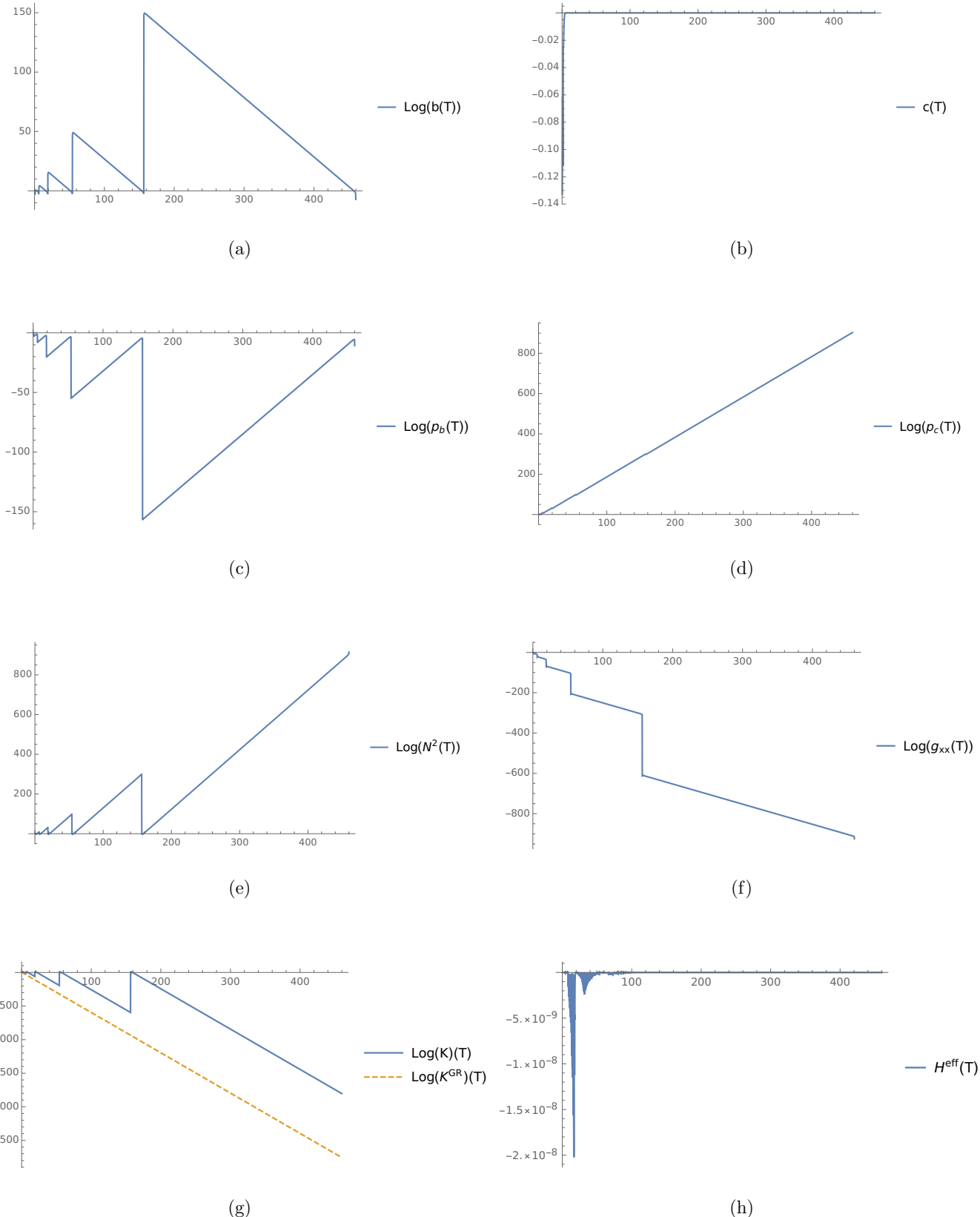


FIG. 1. Plots of the four physical variables (b, c, p_b, p_c) and the effective Hamiltonian defined by Eq.(3.12), together with the metric components N^2 , g_{xx} and the Kretschmann scalar K , as well as the classical counterpart $K^{\text{GR}}(T) \equiv 48m^2/p_c^3$ of $K(T)$. The mass parameter m is chosen as $m/\ell_{pl} = 1$, for which we have $T_T \simeq -1.49$ and $T_H \approx 0.693$. The initial time is chosen at $T_i = 0.3$.

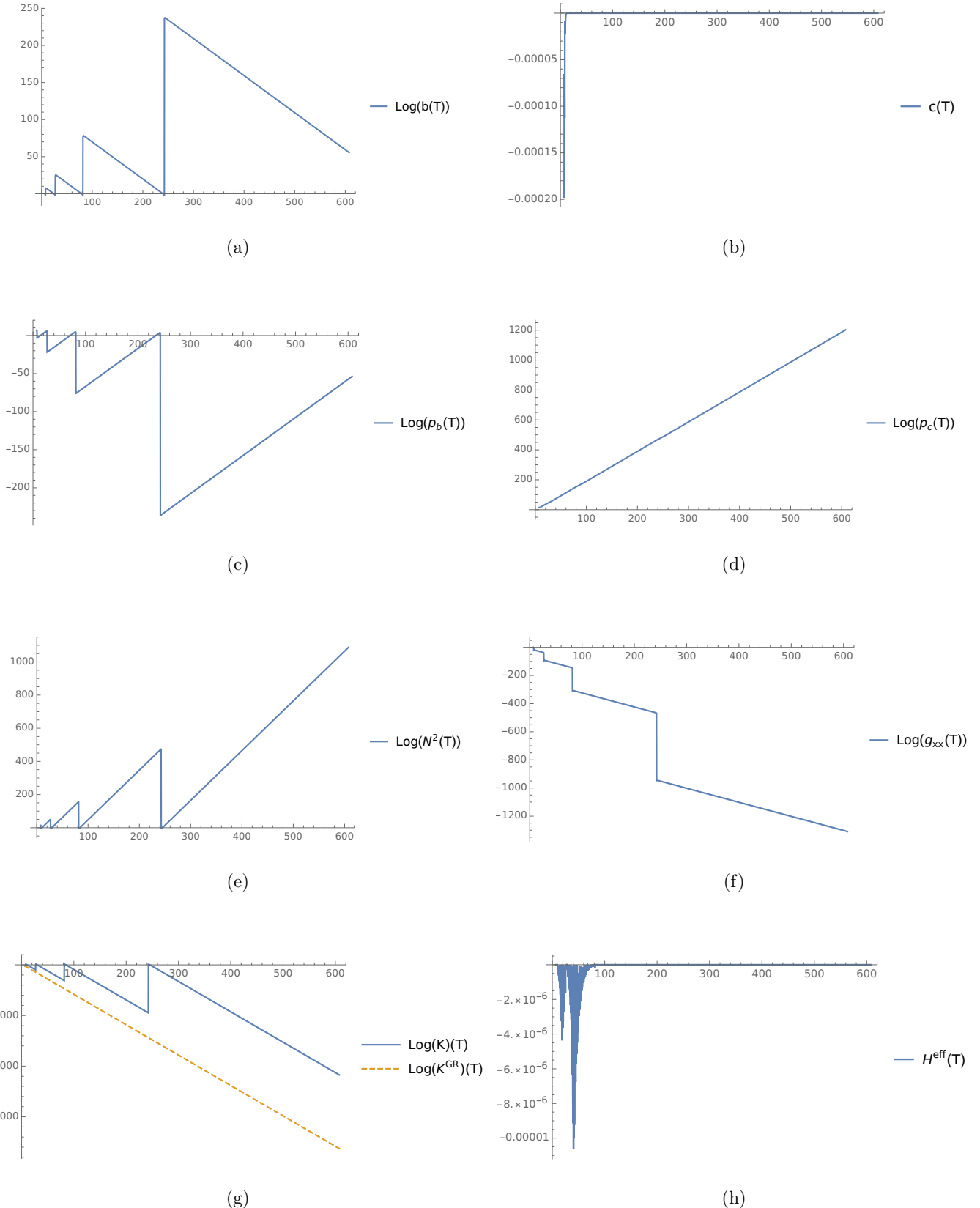


FIG. 2. Plots of the four physical variables (b, c, p_b, p_c) and H^{eff} , together with the metric components N^2 , g_{xx} , the Kretschmann scalar K , and the classical counterpart $K^{\text{GR}}(T) \equiv 48m^2/p_c^3$ with $m/\ell_{pl} = 10^3$, for which we have $T_{\mathcal{T}} \simeq 0.8327$ and $T_H \approx 7.6009$. The initial time is chosen at $T_i = 7.0$.

The above results are sharply in contrast to the classical case, in which $N^2|_{\text{GR}} = e^{2T}/(2me^{-T} - 1) \rightarrow \infty$ at the black hole horizon, $T_H = \ln 2 \simeq 0.693$, while p_b^{GR} becomes zero precisely at T_H , so is g_{xx}^{GR} , as can be seen from Eqs.(2.17) and (2.18).

It should be also noted that similar results can be obtained when the initial time is chosen to be at $T_i = \ln(2m) - 0.05 \simeq 0.643$, which is also a point at which the difference between $c(T_i)$ and $c^{\text{GR}}(T_i)$ is negligible, as shown in Table II. In addition, we also consider the case $m = 10^3 \ell_{pl}$. The corresponding physical quantities are plotted out in Fig. 2. From these figures we can see that the metric coefficients, (N^2, g_{xx}, p_c) are all finite and non-zero for any given finite time T .

It is remarkable to note that our above conclusions that the metric coefficients $g_{\mu\nu}$ and $g^{\mu\nu}$ are not singular at any given finite time T are strongly supported by the analytical results obtained in [38], in which it was shown explicitly that

$$0 < p_b(\tau), p_c(\tau) < \infty, \quad (3.23)$$

for any given finite time τ , where τ denotes the proper time obtained by choosing the lapse function to be unity, $N(\tau) = 1$. Note that in [38] the authors considered space-times filled with matter. However, their results for $p_b(\tau)$ and $p_c(\tau)$ equally hold in the vacuum case. The above results can be understood as follows: From the condition (3.1), we find

$$\delta_c p_b = \sqrt{\Delta p_c}. \quad (3.24)$$

Thus, for any given finite time T , the right-hand side is always finite and non-zero. Then, if $p_b = 0$ at a time, say, T_H , we must have $\delta_c(T_H) = \infty$, which in turn implies that the quantum geometric effects become numerous. As a result, in the reality p_b will be never zero within a finite time. The above arguments are valid not only for the choice $N(\tau) = 1$ adopted in [38], but also for the current choice of the lapse function.

To study further the asymptotic behaviors of the space-times, let us first notice that $\log(N^2)$ and $\log(g_{xx})$ change periodically, but during each period $\log(N^2)$ increases almost linearly, while $\log(g_{xx})$ decreases almost linearly. In contrast, $\log(p_c)$ increases almost linearly all the time [See the analysis to be given below]. So, during each period we can approximate each of them as $F = F_0 T^\alpha$, where we find that

$$N^2 \simeq A_0 e^{3T}, \quad g_{xx} \simeq B_0 e^{-T}, \quad p_c = p_c^{(0)} e^{2T}, \quad (3.25)$$

where A_0 , B_0 and $p_c^{(0)}$ are constants, usually depending on which period we consider, but the slopes remain almost constant. Then, we find that the effective energy-momentum tensor calculated from $\kappa^2 T_{\mu\nu} \equiv G_{\mu\nu}$ can be written in the form

$$\kappa^2 T_{\mu\nu} = \rho u_\mu u_\nu + p_x x_\mu x_\nu + p_\perp (\theta_\mu \theta_\nu + \phi_\mu \phi_\nu) \quad (3.26)$$

with

$$\rho \simeq p_x \simeq \frac{1}{p_c} + \mathcal{O}(e^{-3T}), \quad p_\perp \simeq \mathcal{O}(e^{-3T}), \quad (3.27)$$

where $(u_\mu, x_\mu, \theta_\mu, \phi_\mu)$ are the unit vectors along, respectively, the $(dT, dx, d\theta, d\phi)$ - directions. In addition, we also have

$$R \simeq \frac{2}{p_c}, \quad K \simeq \frac{4}{p_c^2}, \quad C^{\alpha\beta\mu\nu} C_{\alpha\beta\mu\nu} \simeq \frac{4}{3p_c^2}, \quad (3.28)$$

where $C_{\alpha\beta\mu\nu}$ denotes the Weyl tensor. Thus, the space-time becomes asymptotically flat, but with the Kretschmann scalar decreasing as p_c^{-2} , quite similar to the case studied in [14, 52], instead of p_c^{-3} as in the classical case.

2. Non-existence of Black/White Hole Like Horizons

To see if a black or white hole like horizon exists, let us first consider if a *marginally trapped surface* will be developed in the BV model as T (or p_c) increases. To this goal, we can calculate the expansions of the in-going and out-going radially moving light rays [1, 14, 40, 41]. Introducing the unit vectors, $u_\mu \equiv N \delta_\mu^T$ and $s_\mu \equiv \sqrt{g_{xx}} \delta_\mu^x$, we construct two null vectors $\ell_\mu^\pm = (u_\mu \pm s_\mu)/\sqrt{2}$, which define, respectively, the in-going and out-going radially-moving light rays. Then, the expansions of these light rays are given by

$$\Theta_\pm \equiv m^{\mu\nu} \nabla_\mu \ell_\nu^\pm = -\frac{p_{c,T}}{\sqrt{2} N p_c}, \quad (3.29)$$

where $m_{\mu\nu} \equiv g_{\mu\nu} + u_\mu u_\nu - s_\mu s_\nu$.

Note that the existence of a marginally trapped surface can be equally characterized by the vanishing of the norm of the normal vector to the two-spheres, $T, x = \text{Constant}$ [42]. In fact, introducing the normal vector to the surface $\sqrt{p_c} = r_0$

$$N_\mu \equiv \frac{\partial(\sqrt{p_c} - r_0)}{\partial x^\mu} = \frac{p_{c,T}}{2\sqrt{p_c}} \delta_\mu^T, \quad (3.30)$$

where r_0 is a constant, we find

$$N_\lambda N^\lambda = -\frac{p_{c,T}^2}{4N^2 p_c}. \quad (3.31)$$

A marginally trapped surface will be developed when $N_\lambda N^\lambda = 0$, or equivalently $\Theta_\pm = 0$ [1, 14, 40–42]. However, as shown above, the lapse function N always remains finite within a finite time (Recall that classically we have $N^{\text{GR}}(T_H) = \infty$). Thus, a marginally trapped surface can exist only if $p_{c,T} = 0$. From the dynamical equation (3.8), we can see that this is possible only when

$$\delta_c(T) c(T)|_{T=T_{\text{tr}}} = \frac{\pi}{2}. \quad (3.32)$$

In Fig. 3 we plot out this quantity together with the norm, $N^\lambda N_\lambda$, from which we can see clearly that there

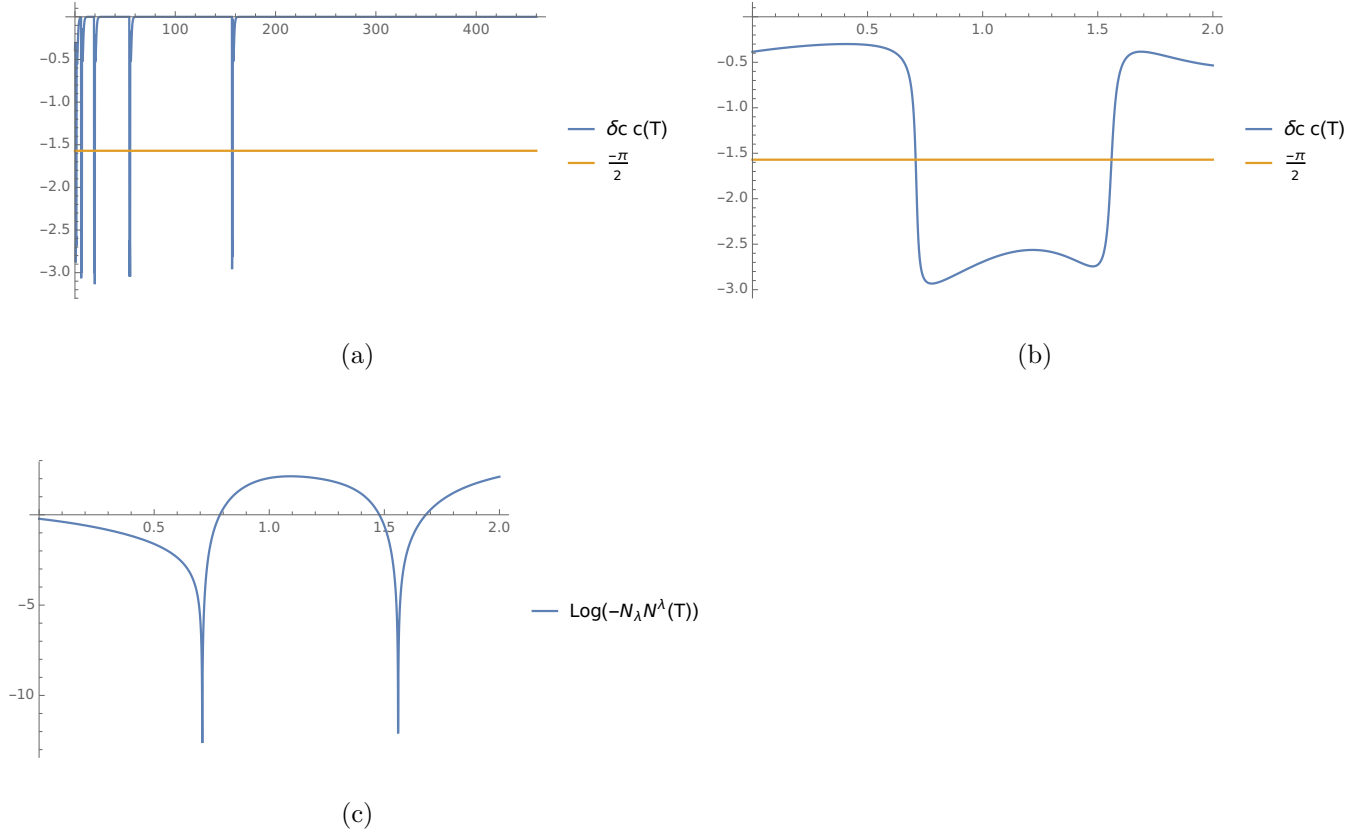


FIG. 3. Plots of $\ln(-N_\lambda N^\lambda)$ defined by Eq.(3.31) and $\delta_c c(T)$. The mass parameter m is chosen as $m/\ell_{pl} = 1$, for which we have $T_\mathcal{T} \simeq -1.49$ and $T_H \approx 0.693$. The initial time is chosen at $T_i = 0.3$. (c) shows clearly that there exist two points at which N^μ becomes a null vector, $N_\lambda N^\lambda = 0$ in the interval $T \in (0, 2)$.

indeed exist various points at which the above condition is satisfied, so that $p_c(T_{\text{tr}}) = 0$ at these points. In particular, in Figs. 3 (b) and (c) we zoom in to the interval $T \in (0, 2)$, which show clearly that two such points exist in this interval, at which $\log(-N^\lambda N_\lambda)$ becomes infinitely large, as N^λ becomes null.

On the other hand, in Fig. 4 we plot several physical quantities for $T \in (0, 2)$ including H^{eff} , which shows $|H^{\text{eff}}| \leq 2.0 \times 10^{-15}$. Therefore, our numerical results are quite reliable in this interval. From this figure, we can see clearly that across these marginally trapped surfaces the metric coefficients all remain finite and non-zero. As a result, these surfaces represent neither black nor white hole horizons, but transition surfaces that separate trapped regions from anti-trapped ones. In fact, across each of these points, $p_{c,T}$ changes its signs. Then, from Eq.(3.29) we can see that both Θ_+ and Θ_- change their signs simultaneously. Therefore, these surfaces always separate trapped regions from anti-trapped ones, while a black (white) hole horizon always separates a trapped region from an untrapped one [1, 40–42]. Therefore, we conclude that *in the BV model, no black/white hole structure exists*.

It should be noted that simply looking at Figs. 1 and 2, one cannot tell the existence of these transition

surfaces. This is because in these figures the quantities are plotted out in such a large range, $T \in (0, 600)$, in which the detailed changes of p_c were washed out, due to the fact that it has quite different values at different times. In particular, the moment $T = 600$ corresponds to $\sqrt{p_c}|_{T=600} \simeq 10^{265}$ m, which is much larger than the size of our current observational universe, $L_{\text{ob.}} \simeq 8.8 \times 10^{26}$ m.

3. Asymptotic Behavior of the Spacetimes as $T \ll T_\mathcal{T}$

To see the connection of our current studies to the ones carried out in [23–25, 37, 39], let us briefly consider the asymptotic behaviors of the spacetimes for $T \ll T_\mathcal{T}$, that is, the asymptotic behaviors of the spacetimes in the pre-transition surface. This can be shown by simply considering the case $m = \ell_{pl}$. With the same initial time and conditions as those chosen for Fig. 1, we plot the four variables $(p_b, b; c, p_c)$ in Fig. 5, from which we can see that they behave very much like the ones obtained in [23–25, 37, 39, 46]. In particular, as T decreases, p_c approaches to a constant \bar{p}_c , which is smaller than the Planck area. Such a spacetime with a constant radius of the two-spheres was first discussed by Nariai [55, 56],

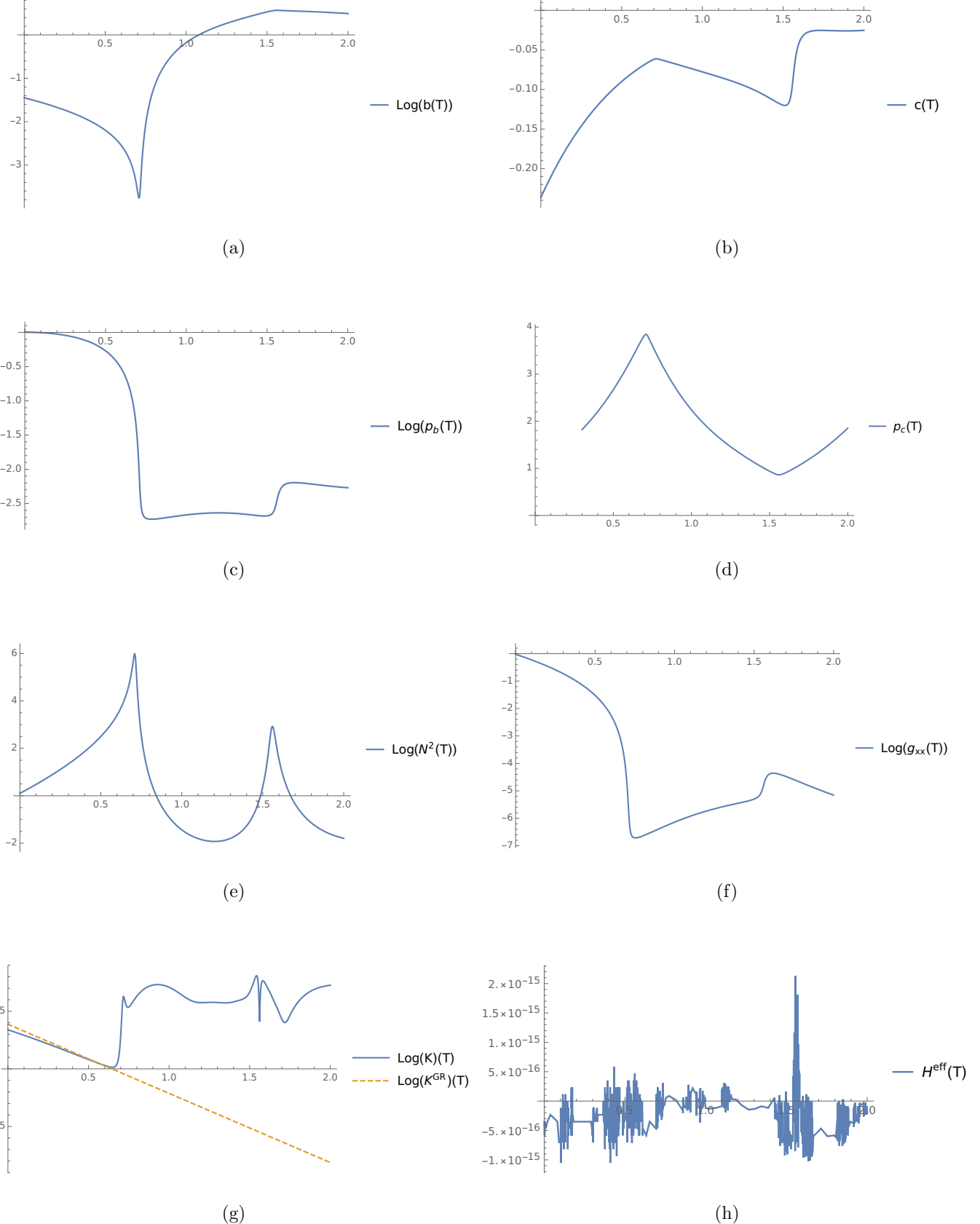


FIG. 4. Plots of the four physical variables (b, c, p_b, p_c) , together with the metric components N^2 , g_{xx} the Kretschmann scalar K , as well as the classical counterpart $K^{\text{GR}}(T) \equiv 48m^2/p_c^3$ of $K(T)$ and H^{eff} in the region $T \in (0, 2)$. The mass parameter m is chosen as $m/\ell_{pl} = 1$, for which we have $T_{\mathcal{T}} \simeq -1.49$ and $T_H \approx 0.693$. The same initial time and conditions are chosen as those of Fig. 1.

and latter generalized to the charged case by Bousso [57]. As shown in detail in [46], in the current case the corresponding solutions are the charged Nariai solutions

$$ds^2 \simeq \left(\frac{\bar{t}_0}{\bar{t}}\right)^2 (-d\bar{t}^2 + d\bar{x}^2) + \bar{p}_c d^2\Omega \\ = -d\bar{t}^2 + e^{2\hat{t}/\bar{t}_0} d\hat{x}^2 + \bar{p}_c d^2\Omega, \quad (3.33)$$

where $d\bar{t} = e^{\bar{\alpha}T} dT$, $\bar{x} = \bar{\beta}x$, and $\bar{\alpha}, \bar{\beta}$ and \bar{t}_0 are all positive constants [46], and $\hat{t} \equiv -\bar{t}_0 \log \bar{t}$, $\hat{x} \equiv \bar{t}_0 \bar{x}$. From the above asymptotic behavior of the metric, we can see that it has a topology of $dS_2 \times S_{(0)}^2$, where $S_{(0)}^2$ denotes a two-spheres with a finite radius. As shown explicitly in [1], the coordinates (\hat{t}, \hat{x}) cover only part of the whole spacetime. After the extension, the corresponding Penrose diagram is that given explicitly in [58].

On the other hand, the Kantowski-Sachs spacetime (2.1) is usually singular in the classical theory, when filled with matter that satisfies certain energy conditions [1]. Then, the corresponding Penrose diagram is given by Fig. 6 (a), in which each point represents a two-sphere with the radius $p_c(T)$ that is a function of T , as shown in Figs. 1 and 2. Note that the horizontal line AB in Fig. 6 (a) represents the spacetime singularity. In the vacuum case, classically it corresponds to $p_c^{\text{GR}}(T = -\infty) = 0$. However, after quantum geometric effects are taken into account, this singularity is replaced by the transition surface \mathcal{T} denoted by the curve APB , and the Penrose diagram for the whole spacetime now is given by Fig. 6 (b). In the past of \mathcal{T} , where $T > T_{\mathcal{T}}$, there actually exist infinite number of such transition surfaces, each of which separates a trapped region from an anti-trapped one. At each transition surface the geometric radius $\sqrt{p_c}(T)$ is different. As T increases, $\sqrt{p_c}(T)$ is getting larger and larger as shown in Figs. 1 and 2. However, in the future of \mathcal{T} , that is, when $T < T_{\mathcal{T}}$, the geometric radius $\sqrt{p_c}(T)$ first gets larger and then gets smaller and smaller, and asymptotically approaches a non-zero constant \bar{p}_c , as shown in Fig. 4 (b).

It must be emphasized that each point in the diagram of Fig. 6 (b) represents two-spheres with different radii. In particular, for $T \ll T_{\mathcal{T}}$, all the two-spheres have the same radius \bar{p}_c , while for $T > T_{\mathcal{T}}$, the radius $p_c(T)$ is time-dependent.

IV. CONCLUSIONS

In this paper, we have studied the quantum effects near the location $T = T_H = \ln(2m)$ at which the classical black hole horizon used to appear within the framework of the improved dynamics approach, first considered by Böhmmer and Vandersloot [23], in which the two polymerization parameters δ_b and δ_c are given by Eq.(3.3), where m is the classical black hole mass. To study such effects, we have chosen the initial conditions as closed to the corresponding classical ones as possible. We have found that this is always possible at a moment T_i , where T_i satisfies the condition $T_{\mathcal{T}} \ll T_i \ll T_H$ [cf. Eqs.(3.18) - (3.20) and Table II], where $T = T_{\mathcal{T}}$ is the location of the (first) transition surface.

To our surprising, we have found that a black hole (or white hole) horizon is never developed within a finite time T to the past of the (first) transition surface $T > T_{\mathcal{T}}$. Instead, only subsequent transition surfaces exist, which always separate trapped regions from anti-trapped ones. The metric coefficients (N^2, g_{xx}, p_c) and their inverses $(N^{-2}, g^{xx}, p_c^{-1})$ are always finite and non-singular at any given finite time T . As a matter of fact, the quantum geometric effects near the classically black hole horizon $T = \ln(2m)$ (at which we have $p_b^{\text{GR}}(T_H) = 0$) are so strong so that $\delta_c(T)|_{T \rightarrow T_H} \gg 1$, as can be seen from Eq.(3.24). Then, in reality p_b never becomes zero within a finite time [38].

These properties are sharply in contrast to those obtained in other models of LQBHs studied so far in LQG [13–17], and put the BV model as a physically viable one of LQBHs questionable.

ACKNOWLEDGMENTS

We would like to thank Prof. Parampreet Singh for valuable discussions and comments, which led to various clarifications and modifications. W-C.G. is supported by Baylor University through the Baylor Physics graduate program. The numerical computations were performed at the public computing service platform provided by TianHe-2 through the Institute for Theoretical Physics & Cosmology, Zhejiang University of Technology. This work is partially supported by the National Natural Science Foundation of China with the Grants No. 11975203, No. 12075202 and No.11875136, and Natural Science Foundation of Jiangsu Province under Grant No. BK20211601.

[1] S. W. Hawking and G. F. R. Ellis, *The Large Scale Structure of Space-Time*, Cambridge Monographs on Mathematical Physics (Cambridge University Press, 2011).

[2] T. Thiemann, *Modern Canonical Quantum General Relativity*, Cambridge Monographs on Mathematical Physics (Cambridge University Press, 2007).

[3] A. Ashtekar and J. Lewandowski, *Class. Quant. Grav.* **21**, R53 (2004), arXiv:gr-qc/0404018.

[4] M. Bojowald, *Phys. Rev. Lett.* **86**, 5227 (2001), arXiv:gr-qc/0102069.

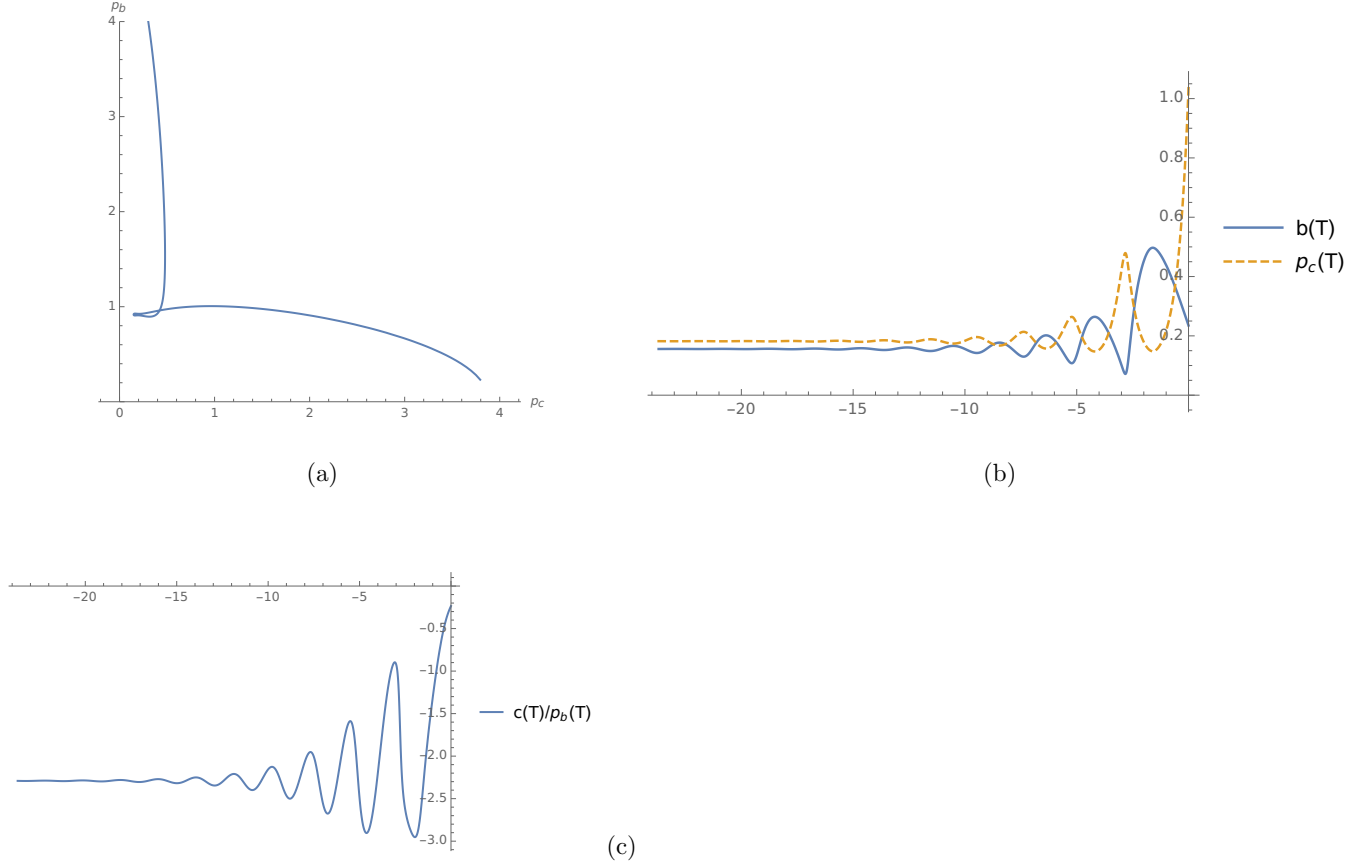


FIG. 5. Plots of the four physical variables (b, c, p_b, p_c) for $T < T_T$ and $m/\ell_{pl} = 1$, for which we have $T_T \simeq -1.49$ and $T_H \approx 0.693$. The same initial time and conditions are chosen as those of Fig. 1.

- [5] M. Bojowald, *Class. Quant. Grav.* **19**, 2717 (2002), [arXiv:gr-qc/0202077](#).
- [6] A. Ashtekar, M. Bojowald, and J. Lewandowski, *Adv. Theor. Math. Phys.* **7**, 233 (2003), [arXiv:gr-qc/0304074](#).
- [7] A. Ashtekar, T. Pawłowski, and P. Singh, *Phys. Rev. D* **74**, 084003 (2006), [arXiv:gr-qc/0607039](#).
- [8] V. Taveras, *Phys. Rev. D* **78**, 064072 (2008), [arXiv:0807.3325 \[gr-qc\]](#).
- [9] A. Ashtekar and P. Singh, *Class. Quant. Grav.* **28**, 213001 (2011), [arXiv:1108.0893 \[gr-qc\]](#).
- [10] W. Kamiński, M. Kolanowski, and J. Lewandowski, *Class. Quant. Grav.* **37**, 095001 (2020), [arXiv:1912.02556 \[gr-qc\]](#).
- [11] P. Singh, *Class. Quant. Grav.* **26**, 125005 (2009), [arXiv:0901.2750 \[gr-qc\]](#).
- [12] A. Corichi and P. Singh, *Phys. Rev. D* **80**, 044024 (2009), [arXiv:0905.4949 \[gr-qc\]](#).
- [13] J. Olmedo, *Universe* **2**, 12 (2016), [arXiv:1606.01429 \[gr-qc\]](#).
- [14] A. Ashtekar, J. Olmedo, and P. Singh, *Phys. Rev. D* **98**, 126003 (2018), [arXiv:1806.02406 \[gr-qc\]](#).
- [15] A. Ashtekar, *Universe* **6**, 21 (2020), [arXiv:2001.08833 \[gr-qc\]](#).
- [16] R. Gambini, J. Olmedo, and J. Pullin, (2022), [arXiv:2211.05621 \[gr-qc\]](#).
- [17] A. Ashtekar, J. Olmedo, and P. Singh, (2023), [arXiv:2301.01309 \[gr-qc\]](#).
- [18] L. Modesto, *Int. J. Theor. Phys.* **45**, 2235 (2006), [arXiv:gr-qc/0411032](#).
- [19] A. Ashtekar and M. Bojowald, *Class. Quant. Grav.* **23**, 391 (2006), [arXiv:gr-qc/0509075](#).
- [20] L. Modesto, *Class. Quant. Grav.* **23**, 5587 (2006), [arXiv:gr-qc/0509078](#).
- [21] A. Corichi and P. Singh, *Class. Quant. Grav.* **33**, 055006 (2016), [arXiv:1506.08015 \[gr-qc\]](#).
- [22] J. Olmedo, S. Saini, and P. Singh, *Class. Quant. Grav.* **34**, 225011 (2017), [arXiv:1707.07333 \[gr-qc\]](#).
- [23] C. G. Boehmer and K. Vandersloot, *Phys. Rev. D* **76**, 104030 (2007), [arXiv:0709.2129 \[gr-qc\]](#).
- [24] D.-W. Chiou, *Phys. Rev. D* **78**, 044019 (2008), [arXiv:0803.3659 \[gr-qc\]](#).
- [25] D.-W. Chiou, *Phys. Rev. D* **78**, 064040 (2008), [arXiv:0807.0665 \[gr-qc\]](#).
- [26] R. Gambini and J. Pullin, *Phys. Rev. Lett.* **110**, 211301 (2013), [arXiv:1302.5265 \[gr-qc\]](#).
- [27] R. Gambini, J. Olmedo, and J. Pullin, *Class. Quant. Grav.* **31**, 095009 (2014), [arXiv:1310.5996 \[gr-qc\]](#).
- [28] R. Gambini, J. Olmedo, and J. Pullin, *Class. Quant. Grav.* **37**, 205012 (2020), [arXiv:2006.01513 \[gr-qc\]](#).
- [29] R. Gambini, J. Olmedo, and J. Pullin, *Front. Astron. Space Sci.* **8**, 74 (2021), [arXiv:2012.14212 \[gr-qc\]](#).
- [30] Y.-C. Liu, J.-X. Feng, F.-W. Shu, and A. Wang, *Phys. Rev. D* **104**, 106001 (2021), [arXiv:2109.02861 \[gr-qc\]](#).
- [31] M. Han and H. Liu, (2022), [arXiv:2212.04605 \[gr-qc\]](#).

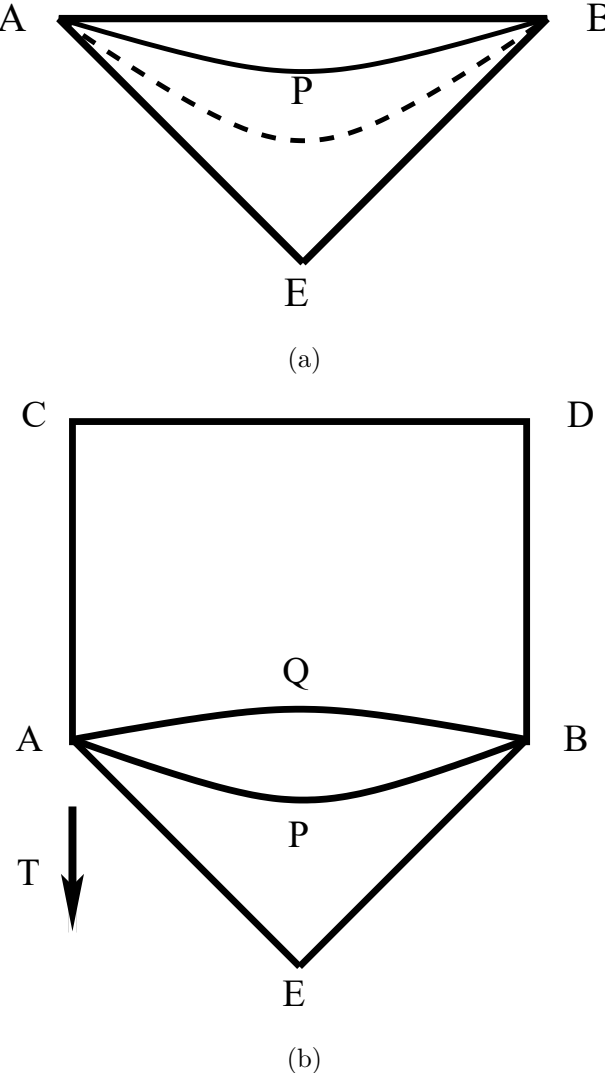


FIG. 6. (a) The Penrose diagram for the Kantowski-Sachs spacetime in classical Einstein's gravity. The horizontal line AB represents the spacetime singularity. In the Schwarzschild case, it corresponds to $p_c^{\text{GR}}(T = -\infty) = 0$. The curve APB corresponds to a $T = \text{Constant}$ surface with a non-zero radius. (b) The Penrose diagram for the BV model. Due to the quantum geometric effects, the classical singularity used to appear at $T = -\infty$ now is replaced by the transition surface T denoted by the curve APB , at which we have $p_c(T_T) > 0$. The quantum geometric effects are large in the region between the two curves AQB and APB . The 2D plane with $\theta, \phi = \text{Constant}$ is asymptotically approaching to a 2D de Sitter spacetime with a fixed radius $\sqrt{p_c}$ as $T \rightarrow -\infty$. In the region $T > T_T$ the spacetime is geodesically complete, and a black (or white) hole like horizon is never developed.

- [32] M. Bojowald, *Class. Quant. Grav.* **21**, 3733 (2004), arXiv:gr-qc/0407017.
- [33] M. Bojowald and R. Swiderski, *Class. Quant. Grav.* **21**, 4881 (2004), arXiv:gr-qc/0407018.
- [34] M. Bojowald and R. Swiderski, *Class. Quant. Grav.* **23**, 2129 (2006), arXiv:gr-qc/0511108.
- [35] M. Campiglia, R. Gambini, and J. Pullin, *Class. Quant. Grav.* **24**, 3649 (2007), arXiv:gr-qc/0703135.
- [36] D.-W. Chiou, W.-T. Ni, and A. Tang, (2012), arXiv:1212.1265 [gr-qc].
- [37] A. Joe and P. Singh, *Class. Quant. Grav.* **32**, 015009 (2015), arXiv:1407.2428 [gr-qc].
- [38] S. Saini and P. Singh, *Class. Quant. Grav.* **33**, 245019 (2016), arXiv:1606.04932 [gr-qc].
- [39] N. Dadhich, A. Joe, and P. Singh, *Class. Quant. Grav.* **32**, 185006 (2015), arXiv:1505.05727 [gr-qc].
- [40] A. Wang, *Gen. Rel. Grav.* **37**, 1919 (2005), arXiv:gr-qc/0309005.
- [41] A. Wang, *Phys. Rev. D* **72**, 108501 (2005), arXiv:gr-qc/0309003.
- [42] Y. Gong and A. Wang, *Phys. Rev. Lett.* **99**, 211301 (2007), arXiv:0704.0793 [hep-th].
- [43] A. Ashtekar, J. Olmedo, and P. Singh, *Phys. Rev. Lett.* **121**, 241301 (2018), arXiv:1806.00648 [gr-qc].
- [44] E. Alesci, S. Bahrami, and D. Pranzetti, *Phys. Lett. B* **797**, 134908 (2019), arXiv:1904.12412 [gr-qc].

- [45] E. Alesci, S. Bahrami, and D. Pranzetti, *Phys. Rev. D* **102**, 066010 (2020), arXiv:2007.06664 [gr-qc].
- [46] W.-C. Gan, G. Ongole, E. Alesci, Y. An, F.-W. Shu, and A. Wang, *Phys. Rev. D* **106**, 126013 (2022), arXiv:2206.07127 [gr-qc].
- [47] L. Modesto, *Int. J. Theor. Phys.* **49**, 1649 (2010), arXiv:0811.2196 [gr-qc].
- [48] J.-M. Yan, Q. Wu, C. Liu, T. Zhu, and A. Wang, *JCAP* **09**, 008 (2022), arXiv:2203.03203 [gr-qc].
- [49] C. Liu, T. Zhu, Q. Wu, K. Jusufi, M. Jamil, M. Azreg-Aïnou, and A. Wang, *Phys. Rev. D* **101**, 084001 (2020), [Erratum: *Phys. Rev. D* 103, 089902 (2021)], arXiv:2003.00477 [gr-qc].
- [50] T. Zhu and A. Wang, *Phys. Rev. D* **102**, 124042 (2020), arXiv:2008.08704 [gr-qc].
- [51] N. Bodendorfer, F. M. Mele, and J. Münch, *Class. Quant. Grav.* **36**, 187001 (2019), arXiv:1902.04032 [gr-qc].
- [52] G. Ongole, H. Zhang, T. Zhu, A. Wang, and B. Wang, *Universe* **8**, 543 (2022), arXiv:2208.10562 [gr-qc].
- [53] A. García-Quismondo and G. A. M. Marugán, *Front. Astron. Space Sci.* **0**, 115 (2021), arXiv:2107.00947 [gr-qc].
- [54] K. A. Meissner, *Class. Quant. Grav.* **21**, 5245 (2004), arXiv:gr-qc/0407052.
- [55] H. Nariai, *General Relativity and Gravitation* **31**, 945 (1999).
- [56] N. Hidekazu, *Sci. Rep. Tohoku Univ. Eighth Ser.* **35**, 46 (1951).
- [57] R. Bousso, *Phys. Rev. D* **55**, 3614 (1997), arXiv:gr-qc/9608053.
- [58] M. Casals, S. R. Dolan, A. C. Ottewill, and B. Wardell, *Phys. Rev. D* **79**, 124043 (2009), arXiv:0903.0395 [gr-qc].